Icarus 227 (2014) 206–209

Contents lists available at ScienceDirect

Icarus

journal homepage: www.elsevier.com/locate/icarus

Note

Formation of Ganymede's grooved terrain by convection-driven resurfacing

Noah P. Hammond *, Amy C. Barr

Department of Geological Sciences, Brown University, Providence, RI 02912, USA

ARTICLE INFO

Article history:
Received 3 July 2013
Revised 20 August 2013
Accepted 21 August 2013
Available online 3 September 2013

Keywords:
Ganymede
Jupiter
Tectonics

ABSTRACT

The heat flux and strain rate inferred for grooved terrain formation on Ganymede can be produced in a convecting ice shell 10–100 km thick with weak near-surface ice. Smooth linear grooves may have formed by convection-driven lithospheric spreading and long-wavelength compressional folds may form atop convective downwellings, and would possibly be detectable with mapping from ESA's upcoming Jupiter-Icy Moon Explorer Mission.

1. Introduction

Over half the surface of Ganymede, Jupiter's largest satellite, is covered in grooved terrain, composed of 10–100 km wide linear and polygonal swaths (Collins et al., 1998) of sub-parallel ridges and troughs (Murchie et al., 1986; Pappalardo, 1998). The ridge and trough spacing is ~7 km, though they are often subdivided by narrower grooves 100 m –1 km wide (Pappalardo, 1998). A subset of groove lanes, which we refer to as "subdued grooves", have straight margins and relatively constant widths over large distances (Head, 2002) and are characterized by subdued light material (Patterson et al., 2010).

Grooved terrain is thought to have formed during an era of global surface expansion (Smith, 1979) resulting from satellite differentiation (Squyres, 1980) or from the melting of the ice I shell when Ganymede entered a possible Laplace-like resonance with Europa and Io (Showman et al., 1997; Bland et al., 2009). Subparallel grooves may form by tilt-block style normal faulting (Pappalardo, 1998) due to tensional stresses in the lithosphere.

Convection in the ice shell has been suggested as a driving mechanism for grooved terrain formation (Lucchitta, 1980; Parmentier et al., 1982), because it can operate globally and generate zones of intense local deformation (Shoemaker et al., 1982). Head (2002) argued that subdued grooves form in a similar way to extensional bands on Europa, which likely form by a convection-driven midocean rift-type mechanism (Prockter et al., 2002).

Previous work argues that convective stresses were not strong enough to drive surface deformation on Ganymede (Squyres and Croft, 1986); convective plumes were thought to be confined below a "stagnant lid", a highly viscous layer of ice which inhibits resurfacing (Solomatov, 1995). However, if the near-surface has a yield stress comparable to the thermal buoyancy stresses from convection, plumes can approach the surface, leading to deformation and efficient heat transport (Trompert and Hansen, 1998; Tackley, 2000; Solomatov, 2004; Showman and Han, 2005). This style of "sluggish lid" convection may be occurring beneath the active South Polar Terrain (SPT) of Enceladus (Barr, 2008). The observed heat flow and surface age of the Enceladus SPT are consistent with heat flows and deformation rates associated with sluggish lid convection (Barr, 2008; Han et al., 2012).

On Ganymede, surface conditions may also have been consistent with sluggish lid convection. Models of flexural uplift estimate a heat flux of 100–200 mW m^{-2} for grooved terrain (Nimmo et al., 2002), and a heat flux of 60–80 mW m^{-2} for the adjacent dark terrain (Nimmo and Pappalardo, 2004). While heat flow estimates based on flexure are somewhat uncertain, independent estimates based on models of groove terrain formation by extensional necking predict a similar heat flux of ~50 mW m^{-2} (Bland et al., 2010). Extensional necking models also predict strain rates between 10^{-16} and 10^{-13} s^{-1} for high-relief grooved material (Dombard and McKinnon, 2001; Bland and Showman, 2007), close to strain rates inferred from folds observed in between the tiger stripes of the SPT (Barr and Preuss, 2010).

Here, we simulate solid-state convection in an ice shell with a weak upper surface to show that the heat flow and deformation rates arising from sluggish lid convection are consistent with the

* Corresponding author. Address: Department of Geological Sciences, Brown University, 324 Brook Street, Box 1846, Providence, RI 02912, USA. Fax: +1 (401) 863 2058.
E-mail address: noah_hammond@brown.edu (N.P. Hammond).

0019-1035/$ - see front matter © 2013 Elsevier Inc. All rights reserved.
http://dx.doi.org/10.1016/j.icarus.2013.08.024

conditions inferred for grooved terrain formation. Subdued grooves may be areas where convection drove complete lithospheric separation, whereas other grooves may form in response to subsurface flow above a convective upwelling (Lucchitta, 1980).

2. Methods

We use the two-dimensional Cartesian finite element model CITCOM (Moresi and Solomatov, 1995) to simulate solid state convection in Ganymede's ice shell. We explore a wide range of ice shell conditions by varying the basal Rayleigh number, Ra_1, which governs the vigor of convection and is related to D, the ice shell thickness,

$$Ra_1 = \frac{\rho g \alpha \Delta T D^3}{\kappa \eta_1}, \quad (1)$$

with ice density $\rho = 1000$ kg m^{-3}, surface gravity $g = 1.4$ m s^{-2}, coefficient of thermal expansion $\alpha = 10^{-4}$ K^{-1}, basal viscosity η_1, thermal diffusivity $\kappa = 10^{-6}$ m^2 s^{-1}, and $\Delta T = 150$ K is the difference between the temperature at the base (260 K) and the surface (110 K) of the ice shell. With these parameters, $Ra_1 = 2.1 \times 10^8 (D/100\text{ km})^3 (10^{14}\text{ Pa s}/\eta_1)$.

We use a simple temperature dependent viscosity (Solomatov and Moresi, 2000), $\eta(T) = \eta_0 \exp(-\gamma T)$, where $\gamma = \theta/\Delta T$, $\theta = \ln(\Delta\eta)$, and $\Delta\eta = \eta_0/\eta_1$ is the viscosity contrast between ice at the surface (η_0), and ice at the base of the shell. On Ganymede, the $\Delta\eta$ predicted for an ice shell deforming by Newtonian volume diffusion is very large (Goldsby and Kohlstedt, 2001), and convection is predicted to occur in the stagnant lid regime. However, the effective viscosity of the surface can be dramatically reduced if convective stresses exceed the lithospheric yield stress (Solomatov, 2004), leading to so-called "sluggish lid" convection. Previous work shows that sluggish lid behavior can occur on Enceladus and Europa for surface yield stress <100 kPa (Showman and Han, 2005; Barr, 2008; O'Neill and Nimmo, 2010). Here, we limit the effective viscosity of surface by imposing a low $\Delta\eta$, which is the simplest way of mimicking the effect of brittle surface ice with a low yield stress (Barr, 2008). We use $\eta_1 = 10^{14}$ Pa s, for an ice grain size ~0.1 mm (Barr and McKinnon, 2007).

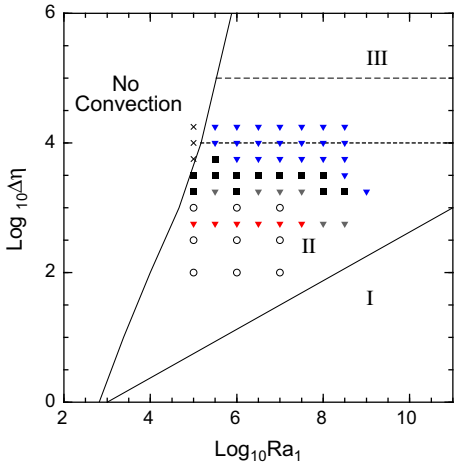

Fig. 1. Values of Rayleigh number (Ra_1) and viscosity contrast ($\Delta\eta$) explored in this study. Black squares represent simulations which successfully match heat flux estimates based on flexure for grooved terrain and dark terrain at strain rates inferred from models of extensional necking. Inverted triangles show simulations that do not meet these criterion, with blue showing those with a heat flow that is too low, gray showing those with an average strain rate exceeding 10^{-13} s^{-1}, and red showing simulations with an average heat flux exceeding 200 mW m^{-2} in regions of extension. "x" symbols show simulations that do not convect and empty circles represent simulations run for the Enceladus SPT by Barr (2008). Lines indicate the boundaries between convective regimes: isoviscous (I), sluggish lid (II), and stagnant lid (III). Dashed lines indicate gradual transition from sluggish lid regime to stagnant lid regime.

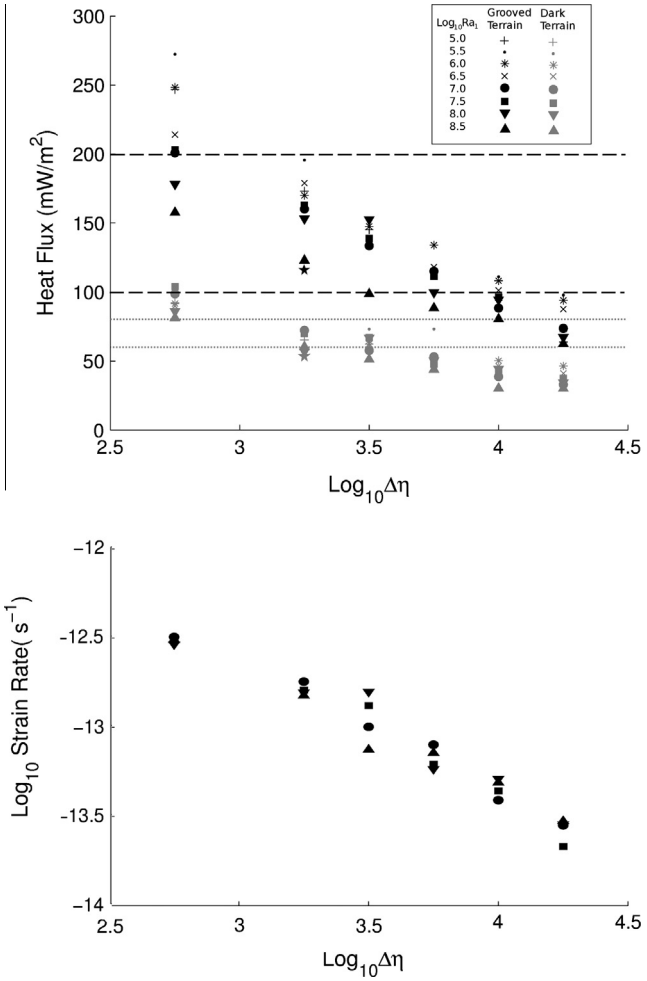

Fig. 2. (top) Heat flux of convection simulations plotted as a function of viscosity contrast. Basal Rayleigh numbers of $\log_{10}(Ra_1) = (5.0, 5.5, 6.0, 6.5, 7.0, 7.5, 8.0, 8.5)$ are plotted with the symbols, (indicated in legend), plus, dot, asterisk, cross, circle, square, inverted triangle and upright triangle, respectively. Star symbols represent one simulation for $Ra_1 = 10^9$. Black symbols represent average heat flux in regions of extension, and gray symbols show the average heat flux in regions of contraction. Black dashed lines show estimated heat flux for grooved terrain. Gray dotted lines show estimate heat flux for dark terrain. (Bottom) Surface strain rate of convection simulations plotted as a function of viscosity contrast. Basal Rayleigh numbers represented by same symbols as above, although many overlap and are not visible.

We simulate convection for $\Delta\eta$ between $10^{2.75}$–$10^{4.25}$, close to the boundary between the sluggish lid regime and stagnant lid regime, $\Delta\eta \sim 10^4$–10^5 (Solomatov, 1995). We model convection in an 8×1 domain, with 512×64 elements, with periodic boundary conditions at the sides to minimize edge effects. We use a basally heated ice shell because the spatial distribution of tidal dissipation in a convecting ice shell is not fully understood (Han and Showman, 2010). Additionally, surface deformation rates and heat flow are likely insensitive to the precise mode of heating (Solomatov and Moresi, 2000). We allow all our simulations to reach a steady state, then measure how strain rate and heat flux vary at the surface.

The convective heat flux, $F = \frac{k\Delta T}{D} Nu$, where $k = 3.3$ W m^{-1} K^{-1} is the thermal conductivity and Nu is the Nusselt number, which describes the efficiency of convective versus conductive heat transport. The strain rate is approximated by $\dot{\varepsilon} = (\partial v_{xsf}/\partial x)$, where v_{xsf}

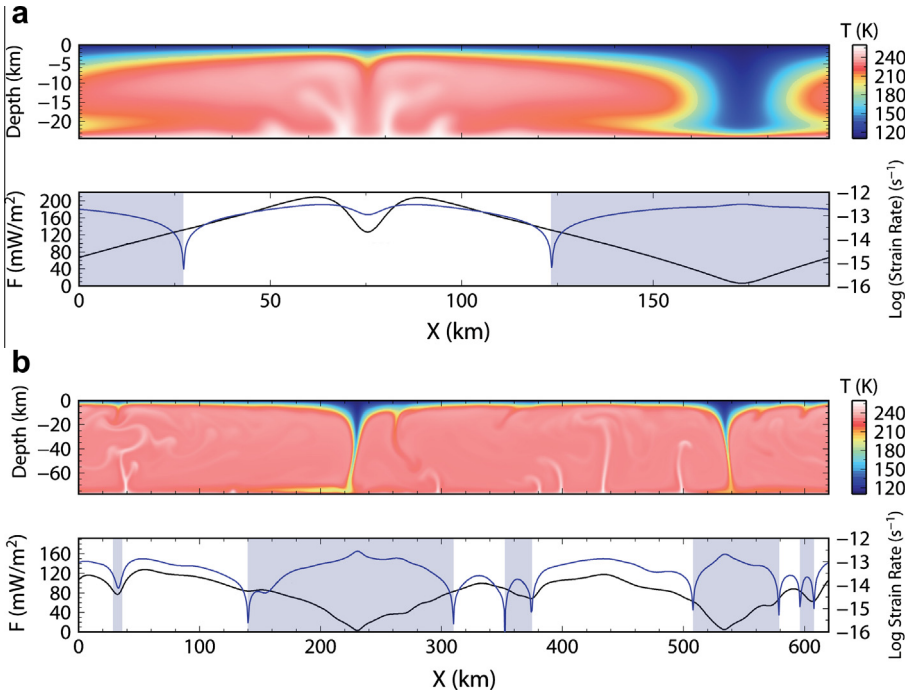

Fig. 3. Temperature fields of convection simulations with the corresponding surface heat flux (black) and strain rate (blue) plotted below. Shaded areas indicate regions of surface contraction interpreted as dark terrain (a) Simulation with $Ra_1 = 10^6$ and $\Delta\eta = 10^{3.25}$, corresponding to $D = 25$ km. A groove lane 150 km wide forms at $x = 75$ km. (b) Simulation with $Ra_1 = 10^8$ and $\Delta\eta = 10^{3.5}$, corresponding to $D = 80$ km. Groove lanes form near $x = 50$ km (80 km wide) and $x = 450$ km (100 km wide). Narrower groove lanes also form near $x = 10$ km, $x = 330$ km and $x = 590$ km.

is the horizontal velocity at the surface. Simulations successfully match the inferred conditions for grooved terrain formation if regions of surface extension have an average heat flux of 100–200 mW m^{-2}, regions of compression have a heat flux of 60–80 mW m^{-2} predicted for dark terrain, and surface strain rates are 10^{-13}–10^{-16} s^{-1}.

3. Results

For $Ra_1 = 10^5$–$10^{8.5}$ and $\Delta\eta = 10^{3.25}$–$10^{3.75}$ (see Fig. 1), convection can match the heat flux inferred for both grooved terrain and dark terrain, at surface strain rates suggested by extensional necking models. Given a basal viscosity of 10^{14} Pa s, ice shell thicknesses of 8–110 km and an effective surface viscosity $\eta_0 < 10^{18}$ Pa s are conducive to forming grooved terrain in a convecting ice shell. This corresponds to a surface yield stress $\sigma_{sy} < 60$ kPa for $\eta_0 \sim \sigma_y(z)/2\dot{\varepsilon}$, with $\sigma_y(z) = \sigma_{sy} + \mu\rho gz$, coefficient of friction $\mu = 0.1$, $\dot{\varepsilon} = 10^{-13}$ s^{-1} and depth $z = 1$ km, close to elastic thickness estimates for grooved terrain (Nimmo et al., 2002).

Fig. 2 shows the surface strain rate and heat flow in regions of extension and contraction as a function of $\Delta\eta$. The average heat flux is independent of Ra_1, however, lower Rayleigh numbers result in larger differences in heat flux over regions of extension and contraction; more vigorously convecting ice shells generate more uniform surface heat flows. For $\Delta\eta \geqslant 10^4$ the surface heat flux is below that inferred from models of flexure, but may be consistent with estimates based on models of extensional necking. Surface strain rates are significant even for $\Delta\eta > 10^{3.75}$, suggesting that convection-driven resurfacing can occur on the boundary between the stagnant lid and sluggish lid regimes. For $\Delta\eta \leqslant 10^{3.25}$ the average surface strain rate exceeds the range inferred from extensional necking models, however strain rates as high as 10^{-12} s^{-1} have been inferred for Europan bands (Stempel et al., 2005), which may be a more appropriate constraint for subdued grooves.

Fig. 3a shows the temperature field, and the variation of F and $\dot{\varepsilon}$ on the surface, of a convection simulation with $Ra_1 = 10^{6.5}$ and $\Delta\eta = 10^{3.25}$, corresponding to $D = 25$ km. Regions undergoing extension are interpreted as sites of groove formation and are ~100 km wide, with an average heat flux of 170 mW m^{-2} and strain rates of 10^{-14}–10^{-13} s^{-1}. Outside this region, the average heat flux is 70 mW m^{-2}. Fig. 3b shows a case with $Ra_1 = 10^8$ and $\Delta\eta = 10^{3.75}$, with $D \sim 80$ km. Here, groove lanes are 20–120 km wide with $F \sim 100$ mW m^{-2} and $F \sim 50$ mW m^{-2} outside this region, just below that inferred for dark terrain. In each successful case, ~50% of the surface is under extension, consistent with proportionality of extensional grooved terrain and dark terrain. Convective downwelling regions remain stationary, allowing for the persistence of relatively undeformed terrain.

4. Discussion

Here we use a simple model to show that sluggish lid convection can provide the heat flux and strain rate inferred for grooved terrain formation. Calculations using more sophisticated plastic rheologies and in a spherical domain are required to test whether convection can create linear groove lanes. Viscosity dependent internal heating modes (e.g. Han and Showman, 2010) and the incorporation of damage or strain weakening (e.g. Buck et al., 2003; Bland et al., 2010) into convection models could be important in localizing surface deformation.

To form grooved terrain by convection, the upper surface must be sufficiently weak to allow convective plumes to come close to the surface. The effective yield stress of ice in tidally flexed ice shells may be low, as suggested by the presence of cycloids on Europa (Hoppa et al., 1999) and locations of tiger stripe plumes on Enceladus (Hurford et al., 2007), which both seem to be controlled by diurnal tidal stresses ~10–100 kPa. Our results suggest a yield stress of this magnitude may permit convection-driven resurfacing, however this may require a coefficient of friction of

ice below the range suggested from laboratory experiments (Schulson and Fortt, 2012). Stresses from global surface expansion, which were likely important (Collins, 2008) may also have increased background extensional stresses and reduced the effective yield stress, allowing convection to drive deformation.

If the total extensional strain on Ganymede exceeds that from global expansion, convection was a likely driving force because passive spreading could not have driven deformation once expansion stresses had been alleviated. Estimates of the strain recorded in grooved terrain depend on the formation mechanism of subdued grooves (Collins, 2006), which could form by lithospheric spreading (Head, 2002) or cyovolcanism (Schenk et al., 2001). Abundant evidence for lithospheric spreading would imply a surface strain beyond what is possible (Collins, 2006) from differentiation and resonance (Squyres, 1980; Bland et al., 2009).

Dark terrain preserved above convective downwelling regions would have experienced significant contraction. Contraction has a variety of surface expressions, but by analogy with Europa, we expect long-wavelength compressional folds to form in the dark terrain (Prockter and Pappalardo, 2000; Pappalardo and Collins, 2005). Bland and McKinnon (2012) show that fold formation and lithospheric thickening on Europa can occur for strain rates of 10^{-12}–10^{-15} s^{-1} and $F \sim 20$–100 mW m^{-2}, close to conditions above convective downwelling regions in our models (see Fig. 3). No contractional features have been observed in dark terrain (Pappalardo et al., 2004) and deformed craters in dark terrain even show evidence for significant surface extension (Pappalardo and Collins, 2005). However, the presence of pervasive, long-wavelength and low-amplitude folds, would allow dark terrain to be regions of net contraction which accommodate extension in grooved terrain. Identification of long wavelength folds in dark terrain and crustal spreading along subdued grooves by ESA's upcoming JUICE mission would support convection-driven grooved terrain formation.

Acknowledgment

This work was supported by NASA Planetary Geology & Geophysics Grant NNX12AI76G.

References

Barr, A.C., 2008. Mobile lid convection beneath Enceladus' south polar terrain. J. Geophys. Res. 113, 7009. http://dx.doi.org/10.1029/2008JE003114.
Barr, A.C., McKinnon, W.B., 2007. Convection in ice I shells and mantles with self-consistent grain size. J. Geophys. Res. 112, 2012. http://dx.doi.org/10.1029/2006JE002781.
Barr, A.C., Preuss, L.J., 2010. On the origin of south polar folds on Enceladus. Icarus 208, 499–503.
Bland, M.T., McKinnon, W.B., 2012. Forming Europa's folds: Strain requirements for the production of large-amplitude deformation. Icarus 221, 694–709.
Bland, M.T., McKinnon, W.B., Showman, A.P., 2010. The effects of strain localization on the formation of Ganymede's grooved terrain. Icarus 210, 396–410.
Bland, M.T., Showman, A.P., 2007. The formation of Ganymede's grooved terrain: Numerical modeling of extensional necking instabilities. Icarus 189, 439–456.
Bland, M.T., Showman, A.P., Tobie, G., 2009. The orbital thermal evolution and global expansion of Ganymede. Icarus 200, 207–221.
Buck, W.R., Lavier, L.L., Babeyko, A., 2003. A numerical model of lithospheric extension producing fault-bounded basins and ranges. Int. Geol. Rev. 45 (8), 712–723.
Collins, G.C., 2006. Global expansion of Ganymede derived from strain measurements in grooved terrain. Lunar Planet. Sci. 39. Abstracts 2077.
Collins, G.C., 2008. Driving mechanisms for grooved terrain formation on Ganymede: Comparison of theory to global groove database. Lunar Planet. Sci. 39, 2254.
Collins, G.C., Head, J.W., Pappalardo, R.T., 1998. Formation of Ganymede grooved terrain by sequential extensional episodes: Implications of Galileo observations for regional stratigraphy. Icarus 135, 345–359.
Dombard, A.J., McKinnon, W.B., 2001. Formation of grooved terrain on Ganymede: Extensional instability mediated by cold, superplastic creep. Icarus 154, 321–336.
Goldsby, D.L., Kohlstedt, D.L., 2001. Superplastic deformation of ice: Experimental observations. J. Geophys. Res. 106, 11017–11030.
Han, L., Showman, A.P., 2010. Coupled convection and tidal dissipation in Europa's ice shell. Icarus 207, 834–844.
Han, L., Tobie, G., Showman, A.P., 2012. The impact of a weak south pole on thermal convection in Enceladus' ice shell. Icarus 218, 320–330.
Head, J. et al., 2002. Evidence for Europa-like tectonic resurfacing styles on Ganymede. Geophys. Res. Lett. 29, 2151. http://dx.doi.org/10.1029/2002GL015961.
Hoppa, G.V., Tufts, B.R., Greenberg, R., Geissler, P.E., 1999. Formation of cycloidal features on Europa. Science 285, 1899–1902.
Hurford, T.A., Helfenstein, P., Hoppa, G.V., Greenberg, R., Bills, B.G., 2007. Eruptions arising from tidally controlled periodic openings of rifts on Enceladus. Nature 447, 292–294.
Lucchitta, B.K., 1980. Grooved terrain on Ganymede. Icarus 44, 481–501.
Moresi, L.-N., Solomatov, V.S., 1995. Numerical investigation of 2D convection with extremely large viscosity variations. Phys. Fluids 7, 2154–2162.
Murchie, S.L., Head, J.W., Helfenstein, P., Plescia, J.B., 1986. Terrain Types and local-scale stratigraphy of grooved terrain on Ganymede. Lunar Planet. Sci. Abstracts XVII. p. 222.
Nimmo, F., Pappalardo, R.T., 2004. Furrow flexure and ancient heat flux on Ganymede. Geophys. Res. Lett. 31, 19701. http://dx.doi.org/10.1029/2004GL020763.
Nimmo, F., Pappalardo, R.T., Giese, B., 2002. Effective elastic thickness and heat flux estimates on Ganymede. Geophys. Res. Lett. 29, 1158. http://dx.doi.org/10.1029/2001GL013976.
O'Neill, C., Nimmo, F., 2010. The role of episodic overturn in generating the surface geology and heat flow on Enceladus. Nat. Geosci. 3, 88–91.
Pappalardo, R.T., Collins, G.C., 2005. Strained craters on Ganymede. J. Struct. Geol. 27, 827–838.
Pappalardo, R.T. et al., 2004. Geology of Ganymede. Cambridge University Press, pp. 363–396.
Pappalardo, R.T. et al., 1998. Grooved terrain on Ganymede: First results from Galileo high-resolution imaging. Icarus 135, 276–302.
Parmentier, E.M., Squyres, S.W., Head, J.W., Allison, M.L., 1982. The tectonics of Ganymede. Nature 295, 290–293.
Patterson, G.W., Collins, G.C., Head, J.W., Pappalardo, R.T., Prockter, L.M., Lucchitta, B.K., Kay, J.P., 2010. Global geological mapping of Ganymede. Icarus 207, 845–867.
Prockter, L.M., Head, J.W., Pappalardo, R.T., Sullivan, R.J., Clifton, A.E., Giese, B., Wagner, R., Neukum, G., 2002. Morphology of Europan bands at high resolution: A mid-ocean ridge-type rift mechanism. J. Geophys. Res. 107, 5028. http://dx.doi.org/10.1029/2000JE001458.
Prockter, L.M., Pappalardo, R.T., 2000. Folds on Europa: Implications for crustal cycling and accommodation of extension. Science 289, 941–944.
Schenk, P.M., McKinnon, W.B., Gwynn, D., Moore, J.M., 2001. Flooding of Ganymede's bright terrains by low-viscosity water-ice lavas. Nature 410, 57–60.
Schulson, E.M., Fortt, A.L., 2012. Friction of ice on ice. J. Geophys. Res. 117, 12204. http://dx.doi.org/10.1029/2012JB009219.
Shoemaker, E., Lucchitta, B., Wilhelms, D., Plescia, J., Squyres, S., 1982. The geology of Ganymede. In Satellites of Jupiter, vol. 1, pp. 435–520.
Showman, A.P., Han, L., 2005. Effects of plasticity on convection in an ice shell: Implications for Europa. Icarus 177, 425–437.
Showman, A.P., Stevenson, D.J., Malhotra, R., 1997. Coupled orbital and thermal evolution of Ganymede. Icarus 129, 367–383.
Smith, B.A., The Voyager 1 Imaging Team, 1979. The Jupiter system through the eyes of Voyager 1. Science 204, 951–957.
Solomatov, V.S., 1995. Scaling of temperature- and stress-dependent viscosity convection. Phys. Fluids 7, 266–274.
Solomatov, V.S., 2004. Initiation of subduction by small-scale convection. J. Geophys. Res. 109, 1412. http://dx.doi.org/10.1029/2003JB002628.
Solomatov, V.S., Moresi, L.-N., 2000. Scaling of time-dependent stagnant lid convection: Application to small-scale convection on Earth and other terrestrial planets. J. Geophys. Res. 105, 21795–21818.
Squyres, S.W., 1980. Volume changes in Ganymede and Callisto and the origin of grooved terrain. Geophys. Res. Lett. 7, 593–596.
Squyres, S.W., Croft, S.K., 1986. The tectonics of icy satellites. In: Satellites. University of Arizona Press, Tucson, AZ, pp. 293–341.
Stempel, M.M., Barr, A.C., Pappalardo, R.T., 2005. Model constraints on the opening rates of bands on Europa. Icarus 177, 297–304.
Tackley, P.J., 2000. Self-consistent generation of tectonic plates in time-dependent, three-dimensional mantle convection simulations. Geochem. Geophys. Geosys. 1, 1021. http://dx.doi.org/10.1029/2000GC000036.
Trompert, R., Hansen, U., 1998. Mantle convection simulations with rheologies that generate plate-like behaviour. Nature 395, 686–689.